Ridge Waveguide Field Description and Application to Directional Couplers*

WILLIAM J. GETSINGER†, MEMBER, IRE

Summary—An approximate determination of the dominant-mode fields in ridge waveguides at all frequencies has been made. Evaluations of the fields along the walls of a commercially standard single-ridge guide having a usable frequency range from 3.75 to 15.0 Gc, and a commercially standard double-ridge guide having a usable frequency range from 4.7 to 11.0 Gc were carried out, and graphs drawn so that the results could be applied to practical situations. The graphs were used to design some ridge-waveguide directional couplers. Both cross-guide and broad-wall couplers were made in single-ridge waveguides and in double-ridge waveguides, using cross sections approximating those of the above commercially available ridge guides. The validity of the field graphs was demonstrated by the close correspondence between measured and predicted coupling for the cross-guide couplers, and by achieving predicted equality of coupling at the band ends for the broad-wall couplers.

I. Introduction

RIDGE waveguide[1,2,3] is used extensively because of its relatively wide single-mode bandwidth. In designing ridge waveguide devices it is often helpful to know the relative values of the dominant-mode field components over the cross section of the ridge guide, especially those fields along the waveguide walls. This paper makes an approximate determination of ridge waveguide fields, describes how they behave with frequency, and presents graphs of the fields along the walls of two commercially available ridge guides. The usefulness of the graphs will be demonstrated by applying them to the design of ridge-waveguide directional couplers. First it is desirable to know how the field components in a ridge waveguide are related among themselves.

II. Relations Among Field Components

Consider a lossless cylindrical waveguide of arbitrary cross section, but whose electromagnetic boundary conditions are invariant under translation in the axial direction. The fields within such a waveguide can be characterized by modes. As a result of separability of the wave equation the variation of the fields of a single mode is found to be exponential in the axial direction and some axially-independent function of the cross-sectional geometry in the transverse direction. Thus, for a given mode, the relative field structure is the same at every cross section. Relations among field components may be found by expanding Maxwell's curl equations

$$\nabla \times E = -jk\eta H$$

$$\nabla \times H = j\frac{k}{\eta}E \tag{1}$$

for exponential variation in the z direction, for instance, and by equating components having the same directions.[4] For a TE wave, E_z is set to zero, and then the following relations can be found:

$$\left.\begin{aligned} \frac{E_x}{H_y} = -\frac{E_y}{H_x} = \eta\frac{k}{k_z} \\ H_z = \frac{j}{k\eta}\left(\frac{\partial E_y}{\partial x} - \frac{\partial E_x}{\partial y}\right) \end{aligned}\right\}. \tag{2}$$

In the above equations, k is the free-space wave number, η is the impedance of free-space, and k_z is the propagation wave number for the mode involved, where propagation is assumed to take place as $e^{j(\omega t - kzz)}$. Also, as a consequence of separability of the wave equation into axial and transverse solutions

$$k_c^2 + k_z^2 = k^2, \tag{3}$$

where k_c is the transverse, or cutoff, wave number.

At the cutoff frequency, the transverse-resonance condition can be imposed on the waveguide. For waveguides appropriately described in rectangular coordinates, this amounts to requiring that k_z and the transverse H fields be zero, as well as the axial E field, and treating the remaining fields as though they were propagating exponentially in a transverse direction, subject to the boundary conditions imposed by the waveguide cross section.

The field conditions for such a waveguide at the cutoff frequency of a TE mode are

$$\left.\begin{aligned} E_z = H_x = H_y = 0 \\ k_z = 0 \\ k^2 = k_c^2 \end{aligned}\right\}. \tag{4}$$

* Received by the PGMTT, July 11, 1961; revised manuscript received September 18, 1961. This work was supported by Air Force Cambridge Research Laboratories, Bedford, Mass., under Contract AF 19(604)-3502.

† Stanford Research Institute, Menlo Park, Calif.

[1] S. B. Cohn, "Properties of ridge waveguide," PROC. IRE, vol. 35, pp. 783–788; August, 1947.

[2] H.-G. Unger, "Die Berechnung von Steghohleitern," *Arch. elekt. Übertragung*, vol. 9, pp. 157–161; April, 1955.

[3] S. Hopfer, "The design of ridge waveguides," IRE TRANS. ON MICROWAVE THEORY AND TECHNIQUES, vol. MTT-3, pp. 20–29; October, 1955.

[4] S. Ramo and J. R. Whinnery, "Fields and Waves in Modern Radio," John Wiley and Sons, Inc., New York, N. Y.; 2nd ed. See sec. 8.02; 1953.

Assume propagation in the positive x direction as $e^{j\omega t-\gamma_n x}$ in either rectangular section of the ridge waveguide, as pictured in Fig. 1, where γ_n is the propagation constant in the x direction of any mode satisfying (4) in the chosen rectangular section at the cutoff frequency. Maxwell's curl equations given in (1), when expanded according to the conditions of (4) and exponential propagation along $+x$, yield the following relation between transverse electric fields in whichever section γ_n applies in Fig. 1

$$E_y = -\frac{\gamma_n}{\gamma_n^2 + k_c^2}\frac{\partial E_x}{\partial y}. \tag{5}$$

For a specified TE mode, propagating down the ridge-guide in the z direction, (2) and (5) can be used to determine all the electric and magnetic field components at any frequency if the y components of electric fields of the contributing tranversely propagating modes are known over the cross section of the guide at the cutoff frequency. The appropriate wave numbers are found from the boundary conditions and use of (3).

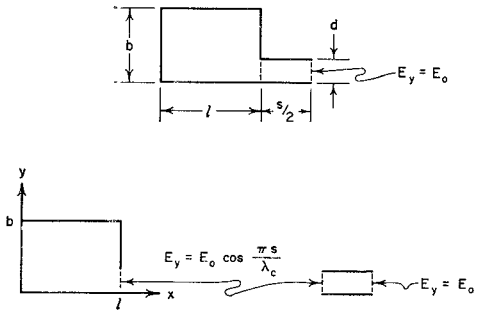

Fig. 1—Equivalent structure analyzed.

III. Derivation of the Waveguide Fields

Cutoff wavelength of a ridge guide is usually found by assuming parallel-plate TEM modes propagating transversely in the separate rectangular sections of the guide cross section, and then forming an equivalent circuit in which these transmission lines are joined by an appropriate lumped-element network representing the effect of the step.[2] While this approach gives good results for cutoff frequency, it does not give a realistic field distribution in the ridge guide, especially in the larger end-sections. On the other hand, an exact field solution is not economically feasible. An approximate solution at the cutoff frequency will be found by assuming a TEM transmission-line mode in the gap, and by matching its electric field at the edge of the ridge to the electric field of a TEM transmission-line mode plus higher order, cutoff TM modes propagating transversely in the large end-sections. In numerical solution, only the first few TM modes will be used. Admittedly, this procedure does not match the magnetic fields, and is inaccurate for all fields very close to the edge of the ridge, but it gives reasonable results elsewhere, and is a great improvement over the assumption of TEM transmission-line modes only.

The model to be analyzed, a half section of a single-ridge guide, is shown in Fig. 1. The electric field will be determined at the cutoff frequency. At the center of the ridge, the electric field is E_0, and exists in the y direction only. Assuming only a TEM transmission-line mode in the gap under the ridge, the electric field at the edge of the ridge for this mode must be

$$\left.\begin{aligned} E_y &= E_0 \cos k_c s/2 \quad 0 < y < d \\ E_y &= 0 \qquad\qquad\quad d < y < b \end{aligned}\right\}. \tag{6}$$

In the larger end-section at the left of Fig. 1, the tangential field is zero along all the inner wall, except at the edge of the ridge where it is given by (6). The parallel plate TEM wave in the end-section is described by

$$E_y = A_0 \sin k_c x. \tag{7}$$

For the cutoff TM waves ($H_x = H_y = 0$), the assumed electric field along x of the nth TM mode has the form

$$E_{xn} = A_n e^{-\gamma_n x} \sin\frac{n\pi y}{b} + B_n e^{\gamma_n x} \sin\frac{n\pi y}{b}, \tag{8}$$

where γ_n is the propagation constant in the x direction for the nth mode, and is used for clarity because k_x would be imaginary for the cutoff TM modes. The following relations hold:

$$\left.\begin{aligned} k_{ny}^2 - \gamma_n^2 &= k_c^2 \\ k_{ny}^2 &= \left(\frac{n\pi}{b}\right)^2 \end{aligned}\right\}. \tag{9}$$

Eq. (9) follows from separability of the wave equation in the rectangular area, bl, of interest.

Eq. (8) is substituted into (5), noting that the sign of (5) must be changed for the waves propagating in a negative x direction, to yield

$$E_{yn} = \frac{\gamma_n}{\gamma_n^2 + k_c^2}\frac{n\pi}{b}\cos\frac{n\pi y}{b}(B_n e^{\gamma_n x} - A_n e^{-\gamma_n x}). \tag{10}$$

But E_{yn} is zero when x is zero, requiring A_n and B_n to be equal. Thus, (8) and (10) become

$$\left.\begin{aligned} E_{xn} &= 2A_n \sin\frac{n\pi y}{b}\cosh\gamma_n x \\ E_{yn} &= 2A_n \frac{\gamma_n}{\gamma_n^2 + k_c^2}\frac{n\pi}{b}\cos\frac{n\pi y}{b}\sinh\gamma_n x \end{aligned}\right\}. \tag{11}$$

The constants A_n are evaluated by imposing the restraints of (6) on the value of the total tangential field E_y at $x = l$. At $x = l$, using (7) and (11),

$$E_y(l) = A_0 \sin k_c l + \sum_{n=1}^{\infty}\frac{2A_n\gamma_n}{\gamma_n^2 + k_c^2}\frac{n\pi}{b}\sinh\gamma_n l\cos\frac{n\pi y}{b}. \tag{12}$$

Eq. (12) is in the form of a cosine series in y, and thus[4] it follows that:

$$\left.\begin{aligned} A_0 \sin k_c l &= \frac{1}{b}\int_0^b E_y(l)\,dy \\ \frac{2A_n\gamma_n}{\gamma_n^2 + k_c^2}\,\frac{n\pi}{b}\sinh\gamma_n l &= \frac{2}{b}\int_0^l E_y(l)\cos\frac{n\pi y}{b}\,dy \end{aligned}\right\}. \quad (13)$$

When (6) has been substituted for $E_y(l)$ in (13), and the integrations are carried out, it is found that

$$\left.\begin{aligned} A_0 &= E_0\,\frac{d\cos k_c s/2}{b\sin k_c l} \\ A_n &= E_0\,\frac{b(\gamma_n^2 + k_c^2)(\cos k_c s/2)(\sin n\pi d/b)}{(n\pi)^2\gamma_n\sinh\gamma_n l} \end{aligned}\right\}. \quad (14)$$

Thus, the fields at the cutoff frequency have been determined, and fields at other frequencies will now be found. Recognizing that

$$\left.\begin{aligned} k &= 2\pi/\lambda \\ k_c &= 2\pi/\lambda_c \\ k_z &= \frac{2\pi}{\lambda}\sqrt{1 - (\lambda/\lambda_c)^2} \end{aligned}\right\}, \quad (15)$$

where λ is free-space wavelength and λ_c is the cutoff wavelength, which can be found from Hopfer's[3] graphs, sufficient information is available to specify approximately all the electric and magnetic fields over the cross section of the ridge guide at any frequency. When the proper substitutions of the equations of this section have been made into the equations of Section II, these fields can be written, for $x<l$, as

$$\left.\begin{aligned} \frac{E_x}{E_0} &= \frac{\eta k}{k_z}\,\frac{H_y}{E_0} = \sum_{n=1}^{\infty}\frac{2b(\gamma_n^2 + k_c^2)}{(n\pi)^2\gamma_n\sinh k_{nx}l}\cos\frac{k_c s}{2}\sin\frac{n\pi d}{b}\cosh\gamma_n x\sin\frac{n\pi y}{b} \\ \frac{E_y}{E_0} &= -\frac{\eta k}{k_z}\,\frac{H_x}{E_0} = \frac{d\cos k_c s/2}{b\sin k_c l}\sin k_c x + \sum_{n=1}^{\infty}\frac{2}{n\pi}\,\frac{\cos k_c s/2}{\sinh\gamma_n l}\sin\frac{n\pi d}{b}\sinh\gamma_n x\cos\frac{n\pi y}{b} \\ -j\frac{\eta k}{k_c}\,\frac{H_z}{E_0} &= (\cos k_c s/2)\left\{\frac{d\cos k_c x}{b\sin k_c l} - \sum_{n=1}^{\infty}\frac{2k_c\sin n\pi d/b}{n\pi\gamma_n\sinh\gamma_n l}\cos\gamma_n x\cos\frac{n\pi y}{b}\right\} \end{aligned}\right\}, \quad (16)$$

and for $l<x<a/2$, as

$$\left.\begin{aligned} \frac{E_x}{E_0} &= \frac{\eta k}{k_z}\,\frac{H_y}{E_0} = 0 \\ \frac{E_y}{E_0} &= -\frac{\eta k}{k_z}\,\frac{H_x}{E_0} = \cos k_c\left(\frac{a}{2} - x\right) \\ -j\frac{\eta k}{k_c}\,\frac{H_z}{E_0} &= \sin k_c\left(\frac{a}{2} - x\right) \end{aligned}\right\}. \quad (17)$$

IV. Ridge Waveguides Used

Commercially available ridge waveguide made of drawn tubing has round corners on the inside cross section. The ridge guides described here have square corners. However, the cross-sectional dimensions were chosen so that the square-cornered guide would approximate electrically a commercially available round-cornered guide.

The single-ridge guide was chosen to be similar to that denoted by the number 50376 in Anderson's paper.[5] Its frequency range is given as 3.75 to 15.0 Gc. The double-ridge guide was chosen to be similar to that denoted by the number ARA-133 in Anderson's paper.[5] This latter guide is more popularly known as DR-19 or D-19, and has a frequency range of 4.7 to 11.0 Gc. The inside cross-sectional dimensions of both the ridge guides used are shown in Fig. 2, along with dimensional ratios and the first two cutoff wavelengths, as computed from Hopfer's[3] curves. The approximate formulas, (16) and (17), for the fields in ridge waveguide were used to compute the relative field values along the inner surfaces of the single-ridge and double-ridge waveguides described in Fig. 2. These fields have been plotted in Fig. 3 for the single-ridge guide and Fig. 4 for the double-ridge guide. Notice that the following definitions have been used:

$$\left.\begin{aligned} e_x &= \frac{E_x}{E_0} & h_x &= -\eta\,\frac{k}{k_z}\,\frac{H_x}{E_0} \\ e_y &= \frac{E_y}{E_0} & h_y &= \eta\,\frac{k}{k_z}\,\frac{H_y}{E_0} \\ & & h_z &= -j\eta\,\frac{k}{k_c}\,\frac{H_z}{E_0} \end{aligned}\right\}. \quad (18)$$

It was found by trial that about five terms of the series expressions in (16) were sufficient to give consistent field representations except very close to the edge of the ridge, although the values used in plotting Figs. 3 and 4 were derived from ten terms.

[5] T. Anderson, "Rectangular and ridge waveguide," IRE Trans. on Microwave Theory and Techniques, vol. MTT-4, pp. 201–209; October, 1956.

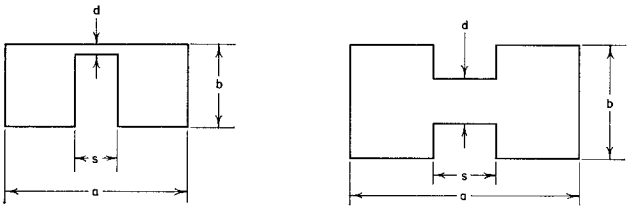

$a=0.813''$	$b/a=0.450$	$a=1.024''$	$b/a=0.500$
$b=0.366''$	$s/a=0.219$	$b=0.512''$	$s/a=0.250$
$d=0.053''$	$d/b=0.145$	$d=0.205''$	$d/b=0.400$
$s=0.178''$		$s=0.256''$	
TE_{10} $\lambda_c=3.70''$	$\lambda_c/a=4.55$	TE_{10} $\lambda_c=2.92''$	$\lambda_c/a=2.85$
TE_{20} $\lambda_c=0.78''$	$\lambda_c/a=0.96$	TE_{20} $\lambda_c=0.95''$	$\lambda_c/a=0.927$

Fig. 2—Dimensions of ridge waveguides used.

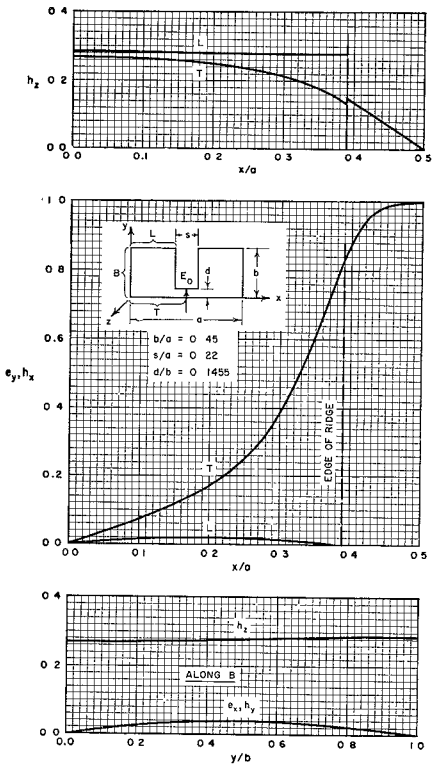

Fig. 3—Peripheral fields—single-ridge guide.

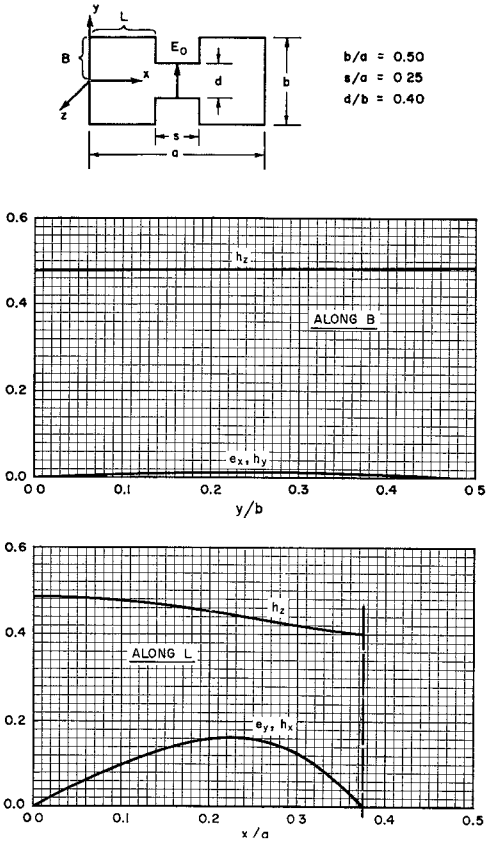

Fig. 4—Peripheral fields—double-ridge guide.

The smooth curve for e_y, h_x in the vicinity of the ridge of the single-ridge guide was achieved by replacing computed values for $0.32<x/a<0.48$ with values taken from a static solution (derived in the Appendix) for the electric field near a right-angle bend near a ground plane. The static solution was used only over a small distance, compared to any wavelength in the guide operating range. The static field faired-in neatly with the dynamic solutions, and thus is believed to be a reasonable approximation to the actual field in the vicinity of the ridge. Inasmuch as a static field has no curl, its use required no change in the computed values of the longitudinal magnetic field h_z. The graph of h_z shows only a small step between the solution under the ridge and the solution of the end-section, and so it is believed that the curve for h_z is a reasonably good approximation to the actual longitudinal magnetic field near the ridge, as well as away from it.

None of the fields of interest in the double-ridge guide was near the gap, and so the computed fields are believed to be reasonably good approximations to actual fields. The usefulness of these curves will be demonstrated by using them in the design of two cross-guide directional couplers and two broad-wall multihole directional couplers.

V. Design of Cross-Guide Couplers

A photograph of the double-ridge cross-guide coupler is reproduced in Fig. 5. The single-ridge cross-guide coupler was made in similar fashion, except that the arms of the crossed slots were aligned with the crossed waveguides. The transmission coefficients A_a and B_a from forward wave in one guide to the forward and backward waves respectively in the other guide are given by Bethe,[6] and, in terms of the quantities of (18), can be written in MKS units as

$$A_a = -\frac{Mh_xh_zk_c}{abs_a} - j\frac{Pe_y{}^2k^2}{2abs_ak_z}$$

$$B_a = -j\frac{Pe_y{}^2k^2}{2abs_ak_z}. \tag{19}$$

The quantities M and P are the magnetic and electric polarizabilities of the aperture. They have been determined experimentally for various aperture shapes by Cohn.[7,8] The term s_a is defined by

$$\frac{S_a}{E_0{}^2} = \frac{ab}{\eta}\frac{k_z}{k}s_a. \tag{20}$$

The quantity S_a is the peak power carried by the waveguide. A rather lengthy expression for power carried by ridge waveguide is given by Hopfer,[3] and will not be repeated here. However, Hopfer's expression has been evaluated for the two ridge guides of Fig. 2. The results can be written as

$s_a = 0.0550$ for the single-ridge guide of Fig. 2

$s_a = 0.1634$ for the double-ridge guide of Fig. 2.

Notice that the dominant term in A_a of (19) is independent of frequency. For the purposes of this paper, a quantity to be called intrinsic attenuation α_i can be defined as

$$\alpha_i = -20\log_{10}|A_a| \text{ db}. \tag{21}$$

The intrinsic attenuation would be the actual coupling for a very small aperture in a very thin wall. Referring to a paper by Cohn,[9] it is possible to take finite slot length and wall thickness into account for the magnetic coupling by defining a frequency-sensitive attenuation factor α_f given by

$$\alpha_f = \frac{54.6tA}{\lambda_a}\sqrt{1-(f/f_a)^2} - 20\log_{10}[1-(f/f_a)^2] \text{ db}. \tag{22}$$

The first term in (22) gives the attenuation due to wall thickness, which is denoted t. The factor A accounts for the interaction of local fields on the two sides of the wall, and has been determined empirically. Quantities f_a and λ_a are the resonant frequency and wavelength of the slot. The length l of a slot of width w is related to its resonant wavelength by the approximate relation

$$l = \frac{\lambda_a}{2} + 0.273w \tag{23}$$

according to Cohn.[9] The second term of (22) gives the change in slot attenuation occurring when the resonant length of the slot becomes an appreciable portion of the wavelength of operation.

Using a value of 2.5 for A, (22) has been plotted as a graph of the frequency-sensitive attenuation factor α_f for various lengths of slots in a wall 0.020 inch thick over the frequency band used by the two ridge guides described previously. The graph is shown in Fig. 6, and although it applies directly to single slots, it is a good approximation for crossed slots, as well. Also, Fig. 6 is not very sensitive to slotwidth. For the worst case, ($l = 0.187$ at 15.0 Gc), it turns out that α_f is about 0.8 db greater for a width of 0.100 inch and about 0.8 db less for a width of 0.025 inch.

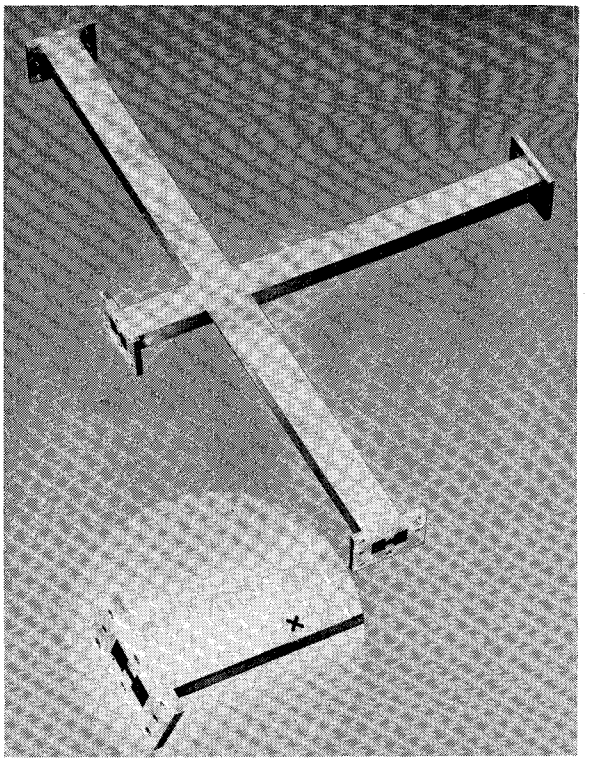

Fig. 5—Photograph of double-ridge cross-guide coupler.

[6] H. A. Bethe, "Theory of Side Windows and Wave Guides," Mass. Inst. Tech. Radiation Lab., Cambridge, Mass., Rept. 43-27; April 4, 1943.

[7] S. B. Cohn, "Determination of aperture parameters by electrolytic-tank measurements," Proc. IRE, vol. 39, pp. 1416–1421; November, 1951.

[8] S. B. Cohn, "The electric polarizability of apertures of arbitrary shape," Proc. IRE, vol. 40, pp. 1069–1071; September, 1952.

[9] S. B. Cohn, "Microwave coupling by large apertures," Proc. IRE, vol. 40, pp. 696–699; June, 1952.

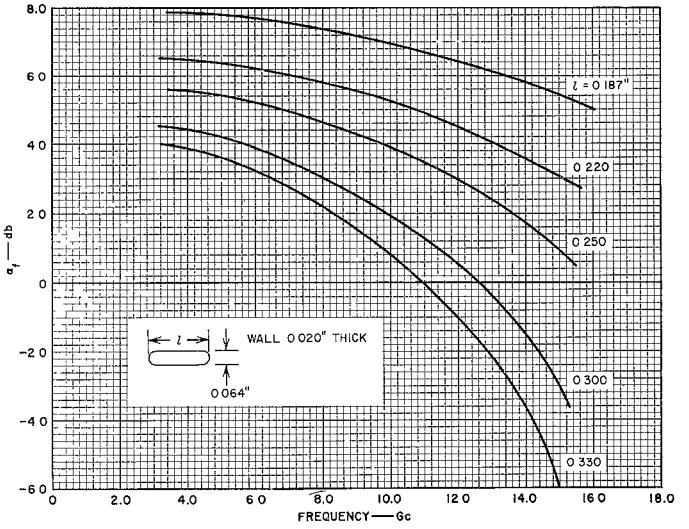

Fig. 6—Attenuation correction for rounded slot of various lengths in 0.020-inch wall.

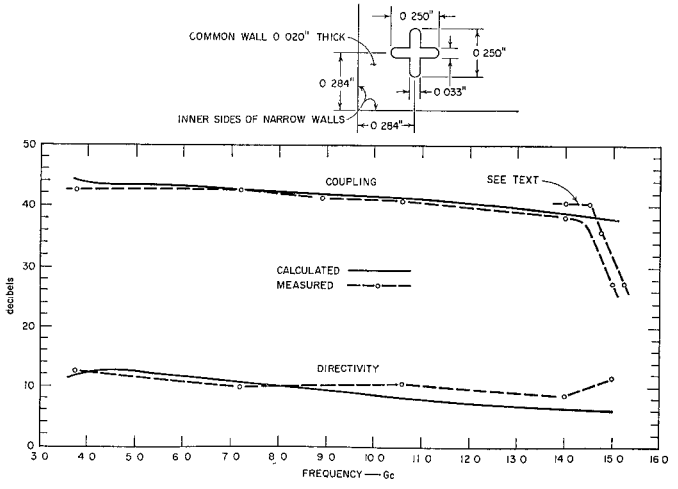

Fig. 7—Performance—single-ridge cross-guide coupler.

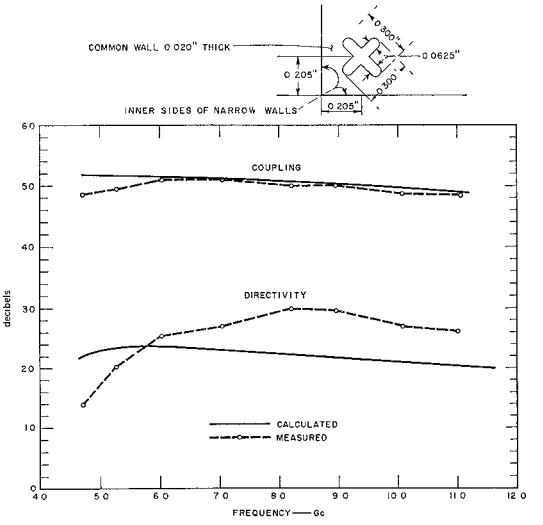

Fig. 8—Performance—double-ridge cross-guide coupler.

The total coupling C, in decibels, of a cross-guide coupler of this type is

$$C = \alpha_i + \alpha_f \text{ db}. \tag{24}$$

The directivity D of the cross-guide coupler is given approximately by

$$D = -20 \log_{10} \left| \frac{B_a}{A_a} \right| \text{db}, \tag{25}$$

where B and A are taken from (19). No correction for wall thickness is included in this definition.

Slot design and performance of a cross-guide coupler in the single-ridge waveguide are shown in Fig. 7. The center of the slot is at $x/a = 0.35$ on the nonridge wall. Agreement between calculated and measured values of coupling is very good up to about 14.5 Gc, where apparently a trapped higher order mode in the ridge guide is generated by the aperture. To illustrate the sudden change of coupling with frequency caused by this trapped mode, a portion of a measured coupling curve for a slightly different aperture is shown in the region of 14 to 15 Gc. The directivity is low because the slot is located at a point of relatively high electric field. The approximate nature of the formula for directivity (26), is indicated by the departure of the calculated curve from the measured curve at the higher frequencies.

A similar coupler using a larger slot was made in the double-ridge guide. Slot design and performance are shown in Fig. 8. This is the same coupler pictured in Fig. 5. The aperture is located at $x/a = 0.20$. The directivity of this coupler is greater than for the single-ridge coupler because the electric field is relatively much smaller at the aperture. The measured and calculated coupling are in good agreement, showing that the field curves, Figs. 3 and 4, gave quite accurate values.

For both couplers the values of e_y, h_x and h_z used are those at the center of the aperture. If the slot lengths are increased in order to obtain more coupled power or improved directivity, then the flatness of coupling deteriorates. If the slot widths are made greater, the directivity deteriorates faster than the coupled power increases. Although suitable only for loose coupling, these couplers can be made to have reasonably flat coupling over the entire range of the ridge guide with adequate directivity for such tasks as power monitoring.

VI. Design of Broad-Wall Couplers

A. General

A photograph of the single-ridge broad-wall coupler is shown in Fig. 9, and a photograph of the double-ridge broad-wall coupler before assembly is shown in Fig. 10. The design principles used for these couplers were similar to those used for multihole couplers[10,11] in rectangular waveguide, and will not be discussed here. However, it will be shown that the field curves of Figs. 3 and 4 can be used to determine the transverse location or orientation of the coupling apertures that gives equal coupling at the ends of the frequency band.

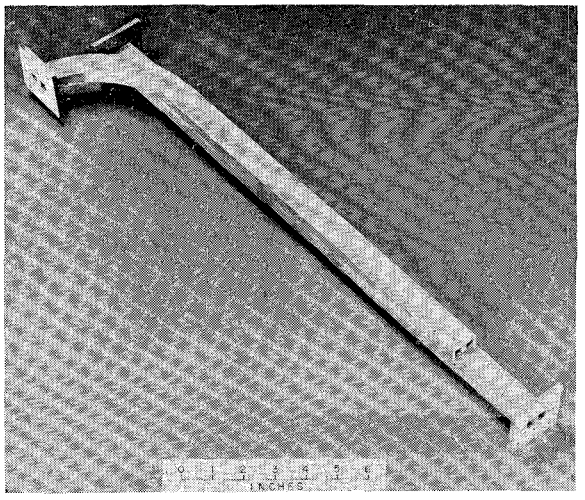

Fig. 9—Photograph of single-ridge broad-wall coupler.

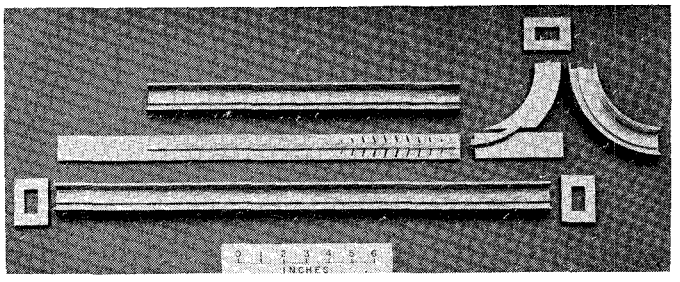

Fig. 10—Photograph of double-ridge broad-wall coupler before assembly.

B. Single-Ridge Coupler

For the single-ridge waveguide, it is practical to use round holes in the nonridged wall. The electric and magnetic polarizabilities of a round hole[12] in a thin wall are

$$\left.\begin{aligned} P &= d^3/12 \\ M &= d^3/6 \end{aligned}\right\}, \tag{26}$$

where d is the hole diameter. However, it is necessary to take into account the variation in coupling with frequency due to wall thickness and aperture diameter.

Using Montgomery's[12] notation, and following Cohn,[9] the fractional attenuations F_E and F_H affecting electric and magnetic field couplings, respectively, are

$$\left.\begin{aligned} F_E &= \frac{\exp\left[-(2\pi t/\lambda_E)\sqrt{1-(f/f_E)^2}\right]}{1-(f/f_E)^2} \\ F_H &= \frac{\exp\left[-(2\pi t/\lambda_H)\sqrt{1-(f/f_H)^2}\right]}{1-(f/f_H)^2} \end{aligned}\right\}, \tag{27}$$

where t is the wall thickness and λ_E and f_E are the cutoff wavelength and frequency of the aperture considered as a waveguide operating in a mode appropriate to the electric field excitation, and λ_H and f_H are the cutoff wavelength and frequency of the aperture operating in a mode appropriate to the magnetic field excitation. For a round hole, the TE_{11} mode applies to the magnetic field and the TM_{01} mode to the electric field. Thus,

$$\left.\begin{aligned} \lambda_E &= 1.305d \\ \lambda_H &= 1.705d \end{aligned}\right\}. \tag{28}$$

A formula for forward transmission through a hole is given by Bethe.[6] Modifying electric field terms by F_E and magnetic field terms by F_H of (27), Bethe's formula can be written as

$$A_a = \frac{jk_c d^3 e_y^2}{12abs_a}\left[\frac{k_z}{k_c}\left(F_H - \frac{F_E}{2}\right) + \frac{k_c}{k_z}\left(\left[\frac{h_z}{e_y}\right]^2 F_H - \frac{F_E}{2}\right)\right]. \tag{29}$$

Equal coupling at the ends of the frequency band is achieved by assuming a "typical" hole diameter in order to determine F_E and F_H at the band ends, and then finding the value of h_z/e_y that causes A_a to be the same at the band ends. For instance, a 0.23-inch round hole in a wall 0.02 inch thick couples equally at 3.75 and

[10] E. F. Barnett and J. K. Hunton, "A precision directional coupler using multi-hole coupling," *Hewlett-Packard J.*, vol. 3, March, 1952; April, 1952.

[11] E. F. Barnett, P. D. Lacy, and B. M. Oliver, "Principles of directional coupling in reciprocal systems," *Proc. Symp. on Modern Advances in Microwave Techniques*, New York, N. Y., November 8–10, 1954, Polytechnic Institute of Brooklyn, New York, July, 1955.

[12] C. G. Montgomery, "Technique of Microwave Measurements," in "Radiation Laboratory Series," McGraw-Hill Book Co., Inc., New York, N. Y., vol. 11, pp. 858–862; 1947.

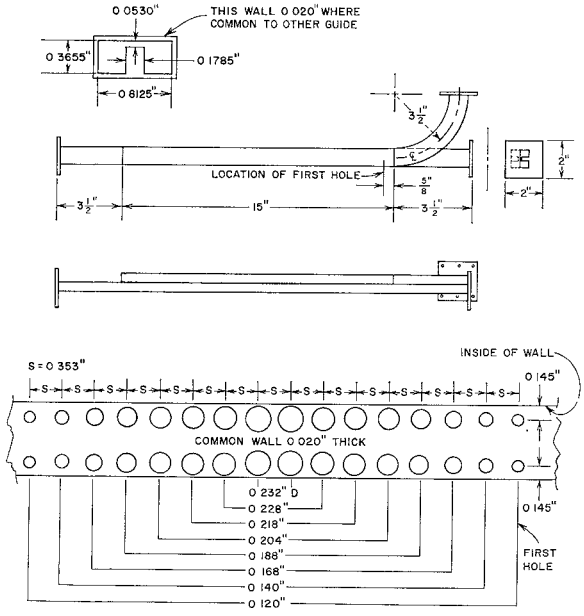

Fig. 11—Pertinent dimensions—single-ridge broad-wall coupler.

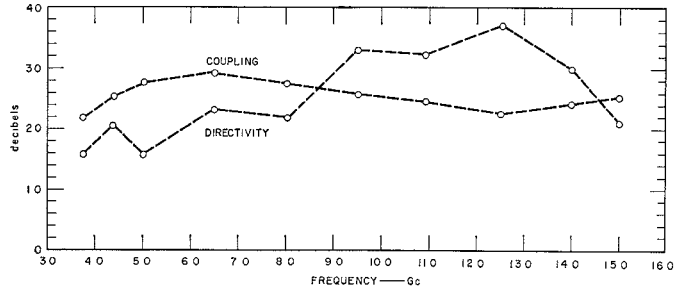

Fig. 12—Performance—single-ridge broad-wall coupler.

15 Gc in the single-ridge guide for $h_z/e_y = 1.76$, which occurs at $x/a = 0.179$ on the graph of Fig. 3.

The single-ridge broad-wall coupler shown in Fig. 9 was originally designed by assuming F_E to be the same as F_H. The coupler made on this basis required the rows of holes to be moved closer to the side walls in order to achieve equal coupling at the band ends. This change would not have been necessary if the coupler had been designed according to the procedure given above. The final dimensions for the coupler are shown in Fig. 11 and its performance is shown in Fig. 12. The coupling curve shows that the location of the holes at $x/a = 0.179$ is fairly close to optimum, based on requiring the same coupling at both ends of the frequency band.

Computations for a Tchebycheff distribution of the aperture coupling showed that 16 holes were sufficient to give 40-db directivity, exclusive of the natural directivity of the individual apertures, and it was on this basis that the coupler was designed. That the directivity achieved was much lower is a measure of the sensitivity of this type of directional coupler to small variations, other than those considered in the analysis, in the electrical characteristics of the guide in the coupling region.

C. Double-Ridge Coupler

The double-ridge broad-wall coupler used narrow tilted slots, as shown in Fig. 10, to achieve equal coupling at the ends of the frequency range. Along the common broad wall of the double-ridge guides the longitudinal magnetic field is much stronger than the transverse magnetic field. Had round holes been used, the coupling would have been much greater at the low-frequency end of the band than at the high-frequency end.

In the practical case it is necessary to make the slots quite long to achieve appreciable coupling. This upsets a number of previously used assumptions. The ends of the slot may be close to both the ridge and the side wall of the waveguide, whereas Bethe[13] assumed the apertures to be far from such walls. The field over the slot is far from uniform, and use of the magnitude of field at the slot center may be an error. These and other factors prevent the accurate prediction of coupling as a function of frequency. Thus, a simplified formula will be given for coupling through a narrow-tilted slot. The best slot angle θ measured with respect to a normal to the wave-

[13] H. A. Bethe, "Lumped Constants for Small Irises," Mass. Inst. Tech. Radiation Lab., Cambridge, Mass., Rept. 43-22; March 24, 1943.

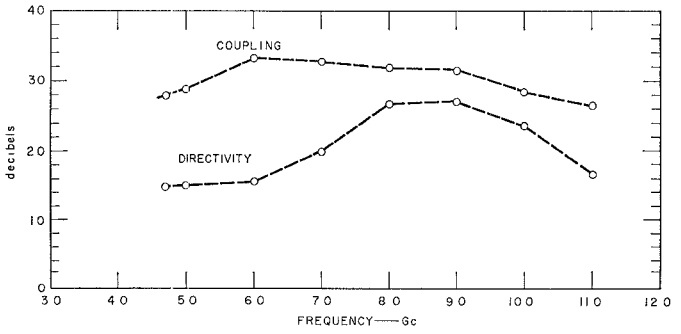

Fig. 13—Performance—double-ridge broad-wall coupler.

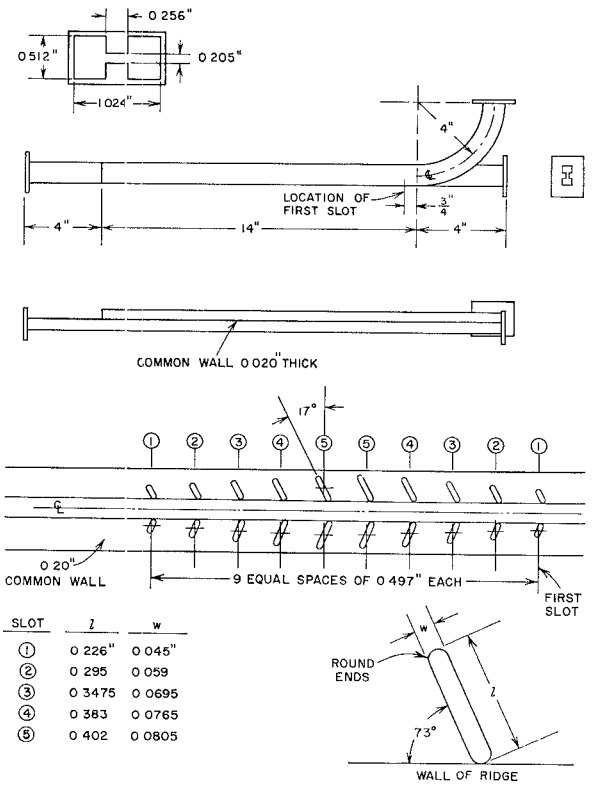

Fig. 14—Pertinent dimensions—double-ridge broad-wall coupler.

guide axis, can be determined approximately by setting the couplings equal at the two ends of the frequency band and solving for θ. The simplified coupling formula is

$$A_a = \frac{jk_c M_l h_x^2 \cos^2\theta}{2abs_a}\left[\frac{k_z}{k_c} + \frac{k_c h_z^2}{h_z h_x^2}\left(\tan^2\theta + \frac{M_t}{M_l}\right)\right], \quad (30)$$

where the transverse magnetic polarizability M_t for a narrow slot is given by Bethe,[13] and can be written as

$$M_t/l^3 = \frac{\pi}{16}\left(\frac{w}{l}\right)^2. \quad (31)$$

For example, in the double-ridge guide, for a slot of $w/l = 0.20$ located at $x/a = 0.19$, giving $(h_z/h_x)^2 = 8.65$ and $M_t/M_l = 0.098$, the solution for equal coupling at 4.7 and 11.0 Gc, according to (30), is $\theta = 15.3°$. The measured performance of the coupler of Fig. 10, which has $\theta = 17°$, is shown in Fig. 13. A small increase in θ would cause a significant increase in coupled power at the lower-frequency end of the band and very little increase at the higher-frequency end. Such a change could be predicted by (30), which also can be used to give individual slot coupling to within a few decibels at some mid-band frequency.

The pertinent details of the double-ridge broad-wall coupler constructed are shown in Fig. 14. This coupler was designed for 30-db coupling and 40-db directivity, using two rows of ten apertures each in a Tchebycheff distribution. The measured coupling, shown in Fig. 13, is reasonably flat over the band. The directivity is lower than the directivity of the single-ridge broad-wall coupler because the apertures are larger and there are fewer of them. Comments made in connection with the directivity of the single-ridge broad-wall coupler apply to the double-ridge broad-wall coupler, also.

Appendix

Determination of Static-Electric Field Near a Corner

Referring to the z plane on Fig. 15, it is desired to find the magnitude of the static-electric field along conductor DEF in the region opposing the corner B on conductor ABC, which is held at a different potential.

The space between conductors on the z plane is mapped onto the upper half of a z_1 plane by

$$z = 2\sqrt{z_1 + 1} + \ln \frac{\sqrt{z_1 + 1} - 1}{\sqrt{z_1 + 1} + 1}, \tag{32}$$

which is taken from Churchill.[14] The upper half z_1 plane is further transformed to the region between parallel plates on the w plane by

$$z_1 = e^{\pi w}. \tag{33}$$

The z_1 plane and w plane are also shown in Fig. 15. Now, the field is uniform on the w plane, and the field on the z plane can be written[15]

$$E = \left| \frac{dw(z)}{dz} \right| = \left| \frac{dw}{dz_1} \frac{dz_1}{dz} \right|. \tag{34}$$

Differentiating (32) and (33) and substituting in (34) yields

$$E = \left| \frac{1}{\pi\sqrt{z_1 + 1}} \right|. \tag{35}$$

For z real ($z_1 > 0$), (35) can be introduced into (32) to give, after manipulation,

$$z = \frac{2}{\pi E} - 2 \text{ arc tanh } \pi E. \tag{36}$$

Eq. (36) assumes unit voltage across the gap π high on the z plane. At $z = -\infty$ the electric field $E(-\infty)$ must have the value $1/\pi$. Thus (36) may be written as

$$z = \frac{2}{e} - 2 \text{ arc tanh } e, \tag{37}$$

where

$$e = \frac{E(z)}{E(-\infty)} \quad (z \text{ real}). \tag{38}$$

[14] R. V. Churchill, "Introduction to Complex Variables and Applications," McGraw-Hill Book Co., Inc., New York, N. Y. See Fig. 27, p. 211; 1948.

[15] W. R. Smythe, "Static and Dynamic Electricity," McGraw-Hill Book Co., Inc., New York, N. Y., ch. IV, 1939.

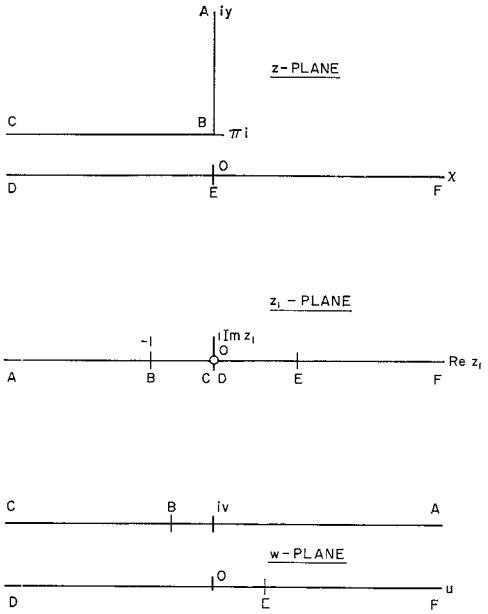

Fig. 15—Mappings for static field determination.

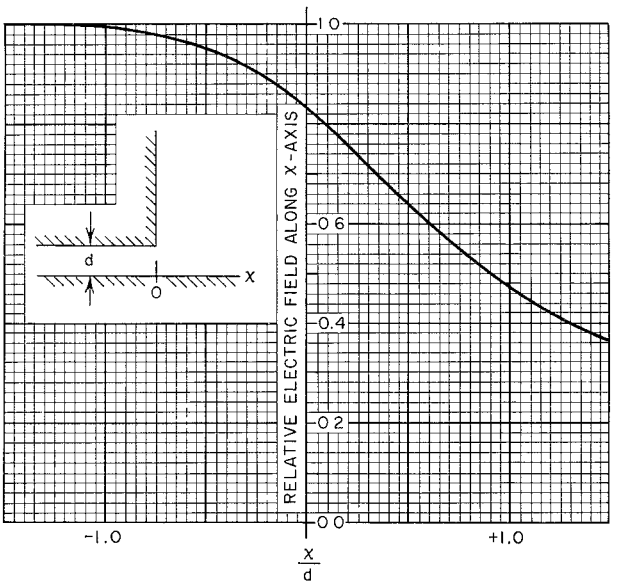

Fig. 16—Relative electric field along wall opposing corner

Finally, transforming to an x plane where the gap is of height, d, rather than π, gives

$$x/d = \frac{2}{\pi}\left(\frac{1}{e} - \text{arc tanh } e\right). \tag{39}$$

Numerical substitution for e in (39) yields the graph shown in Fig. 16.

Acknowledgment

The author wishes to thank E. D. Sharp for his very helpful technical advice during the course of this work.